

# A Combined Experimental and Theoretical Investigation on Organic Cation Dichlorocopper (II): Structural Characterization, Hirshfeld Surface Analysis, Spectroscopic Properties and DFT Calculation

Salah N<sup>1\*</sup>, Samet A<sup>2</sup>, Hamdi B<sup>1</sup> and Ben Salah A<sup>1</sup>

<sup>1</sup>Laboratory of Materials Science and Environment, Faculty of Sciences of Sfax, University of Sfax, 3000 Sfax, Tunisia

<sup>2</sup>Laboratory of Applied Physics, Faculty of Sciences of Sfax, University of Sfax, 3000 Sfax, Tunisia

## Abstract

The (ethylenediamine) dichlorocopper(II) complex,  $\{[\text{Cu}(\text{en})\text{Cl}_2]_n\}(\text{en}:\text{C}_2\text{H}_8\text{N}_2)$ , was synthesized by hydrothermal technique. The X-ray structure of  $\{[\text{Cu}(\text{en})\text{Cl}_2]_n\}$  shows that the compound crystallizes as a one dimensional chain with one chlorine that is non-bridging and the other chlorine which is triply bridging. It crystallizes at room temperature in the centrosymmetric space group  $P2_1/m$ . The structure of  $\{\text{Cu}(\text{en})\text{Cl}_2\}_n$  was originally reported by Kumara et al. The surrounding copper is best described as distorted octahedral. The crystal structure was stabilized with an extensive network of N-H...Cl classical hydrogen bond interactions. The investigation on that close intermolecular interactions between the molecules via Hirshfeld surface analyses is presented to reveal subtle differences and similarities in the crystal structures. The decomposition of the fingerprint plot area provides a percentage of each intermolecular interaction, allowing for a quantified analysis of close contacts within the crystal. The optimized molecular structure and vibrational spectra were calculated by the Density Functional Theory (DFT) method using the B3LYP function with the LanL2DZ basis set. Good consistency is found between the calculated results and the experimental structure, FT-IR, and FT-Raman spectra. The detailed interpretation of the vibrational modes was carried out. Optical transmission measurements performed on thin films of  $\{[\text{Cu}(\text{en})\text{Cl}_2]_n\}$  revealed two absorption bands at 3.64 eV and 1.907 eV. The calculated HOMO-LUMO energies reveal that charge transfer occurs within the molecule.

**Keywords:** Synthesis hydrothermal; Crystal structure; Complex copper (II); Hirshfeld surface analysis; DFT vibrational assignment; Optical absorption

## Introduction

Inorganic-organic hybrid complexes based on metal centre and multifunctional ligands have been perceived as extremely interesting and significant referring materials for not only to their intriguing architectures, but also to their important properties such as electronic [1,2], magnetic [3-6] and optic [3,7]. Inorganic materials, typically characterized by covalent and ionic interactions, offer the potential for high electrical mobility, a wide range of band gaps (enabling the design of insulators, semiconductors, metals, and superconductors), interesting magnetic interactions, a big variety of dielectric properties, substantial mechanical hardness and thermal stability [2,8]. Organic molecules provide the possibility of structural diversity, highly-efficient luminescence, a large degree of polarizability and plastic mechanical properties [9].

Furthermore, hybrid compounds based on copper have been paid special attention to develop a variety of low cost electronic devices. This refers basically to their diverse structures and novel thermochromic, optical and electronic properties [10-15]. The Cu(II) ion, being  $d^9$ , displays a variety of coordination number and geometry depending on the crystal packing and ligand. It has been shown that their structures can vary considerably, ranging from systems based on isolated (0-D) inorganic polyhedra [11,16] to the ones (1-D) containing extended chains as in  $\{(\text{ampyH})_2[\text{Cu}(\text{mal})_2]_n\}$  [17],  $\{(\text{TPPB})\text{CuCl}_2\}_n$  [18],  $[\text{Cu}(\text{phen})(\text{l-ura})(\text{H}_2\text{O})]_n \cdot \text{H}_2\text{O}$  and  $[\text{Cu}(\text{phen})(\text{l-ura})(\text{H}_2\text{O})]_n \cdot \text{CH}_3\text{OH}$  [19] to two-dimensional (2-D) networks [20,21] and right up to three dimensional (3-D) networks as in  $(\text{C}_{10}\text{H}_{26}\text{N}_4)_2 \text{Cl CuCl}_5 \cdot 3\text{H}_2\text{O}$  and  $(\text{H}_2\text{mela})_2[\text{CuCl}_5]\text{Cl}$  [22,23].

The supramolecular assembly is framed by suitable combination of various types of weak intermolecular interactions like N-H...Cl. To explore the intermolecular interactions inside the supramolecular

assembly, it is crucial to obtain quantitative measurements of these interactions. Hirshfeld surface analysis is becoming a valuable tool for elucidating molecular crystal structures quantitatively. In this context, we hereby report the crystal structures and Hirshfeld surface analysis of  $\{[\text{Cu}(\text{en})\text{Cl}_2]_n\}$ . The structure of  $\{\text{Cu}(\text{en})\text{Cl}_2\}_n$  was originally reported by Kumara et al. [24]. With the aim of a deeper understanding the electronic structures of the complex, and related experimental observations, density functional theory (DFT) calculations were performed. The electrostatic potential (ESP), total electron density (ED), molecular electrostatic potential (MEP), Mulliken analysis and frontier molecular orbitals (FMOs) were also studied using the DFT level by means of the B3LYP functional with the LanL2DZ basis set, to obtain adequate information about the electronic characteristics.

## Experimental Methods

### Synthesis of $\{[\text{Cu}(\text{en})\text{Cl}_2]_n\}$ compound

This compound was synthesized under hydrothermal conditions, by mixing  $\text{CuCl}_2 \cdot 2\text{H}_2\text{O}$  (0.172 g) and ethylenediamine (en) (0.5 ml). Both compounds were dissolved in water (5 mL) and stirred at room temperature for 2 h to homogeneity. When the pH value of the mixture

**\*Corresponding author:** Najet Salah, Laboratory of Materials Science and Environment, Faculty of Sciences of Sfax, University of Sfax, 3000 Sfax, Tunisia, Tel: +21674242951; E-mail: najetsalah@yahoo.com

**Received** September 06, 2016; **Accepted** December 13, 2016; **Published** December 19, 2016

**Citation:** Salah N, Samet A, Hamdi B, Salah BA (2016) A Combined Experimental and Theoretical Investigation on Organic Cation Dichlorocopper (II): Structural Characterization, Hirshfeld Surface Analysis, Spectroscopic Properties and DFT Calculation. Chem Sci J 7: 147. doi: 10.4172/2150-3494.1000147

**Copyright:** © 2016 Salah N, et al. This is an open-access article distributed under the terms of the Creative Commons Attribution License, which permits unrestricted use, distribution, and reproduction in any medium, provided the original author and source are credited.

was adjusted to 7.3 by adding 6 mol<sup>-1</sup> NaOH, the cloudy solution was transferred and sealed in a 15 ml Teflon-lined stainless steel autoclave and kept under an autogenous pressure at 160°C for 72 h. After slow cooling to room temperature at a rate of 5°C h<sup>-1</sup>, blue crystals were obtained, which were subsequently filtered, washed with acetone and dried in desiccators at room temperature. A single crystal suitable for X-ray diffraction analysis was selected and studied.

### Crystal data and structure determination

A blue crystal with approximate dimensions 0.51 × 0.32 × 0.2 mm<sup>3</sup> of the Cu-complex was selected after examination with a polarizing microscope (Figure S1). X-ray data were collected at 293(2) K with a KAPPA APEX II automatic diffractometer using Mo K $\alpha$  radiation ( $\lambda=0.71073$  Å). In the range of 2.49 <  $\theta$  < 26.03°, 3232 integrated reflections were collected, reducing to a data set of 694 unique with  $R_{int}=0.0214$ . The structure was solved by direct methods with SHELXS-97 program [25], and refined by the full-matrix least-squares technique against  $F^2$  in anisotropic (for non-hydrogen atoms) with SHELXL-97 program [26]. The hydrogen atoms were refined isotropically. The corrections for absorption were based on multi-scan. Details of this refinement are given in Table 1. The last cycle of refinement included the atomic coordinates for all the atoms, anisotropic thermal parameters and isotropic thermal and factors of anisotropic thermal agitation, the values of which are listed in Tables S1 and S2. The crystal structure and packing diagram were created with Mercury [27] and crystal Maker [28].

### Spectroscopic characterization

The FT-IR spectra were recorded in the 400-4000 cm<sup>-1</sup> region on a Perkin-Elmer Spectrum 100 FT-IR spectrometer with samples as KBr disks at room temperature. The FT-Raman spectrum was measured with a LABRAMHR 800 triple monochromator in the 4000-50 cm<sup>-1</sup> region.

Thin films of  $\{[Cu(en)Cl_2]_n\}$  were prepared by spin coating, on glass slides, in aqueous solution of 20 mg of the crystallized title compound. The film was then annealed at 60°C for 20 min to remove residual solvent. The room temperature absorption spectrum of the spin coated film was recorded using UV-visible Spectrophotometer (Thermoscientific Evolution 60s UV-Visible Spectrophotometer).

### Computational details

The molecular geometry optimizations and vibrational frequency calculations were performed with the Gaussian 03 package [29]. The geometry optimizations for an appropriate cluster model were performed at the DFT level by means of the B3LYP functional [30] with the LanL2DZ basis set [31,32]. The geometry taken from the starting structure was based on the crystallographic data listed in Table 1. Prior to compare the calculated vibrational wavenumbers with the experimental counterparts, the former has been scaled by 0.963 scaling factor [33] to correct the evaluated wavenumbers for vibrational anharmonicity and deficiencies inherent to the used computational level. The Gauss view program [34] was employed to generate visual presentations and verify the normal mode assignments.

### Hirshfeld surface analysis

Hirshfeld surfaces and their associated fingerprint plots were calculated using Crystal Explorer (Version 3.0) software, which accepts a structure input file in the CIF format [35]. For each point on the Hirshfeld isosurface, two distances ( $d_e$ ,  $d_i$ ) are defined. First,  $d_e$ : the distance from the point to the nearest nucleus external to the surface. Second,  $d_i$ : the distance to the nearest nucleus internal to the surface.

The normalized contact distance  $d_{norm}$  based on  $d_e$  and  $d_i$  is given by the following Eq 1:

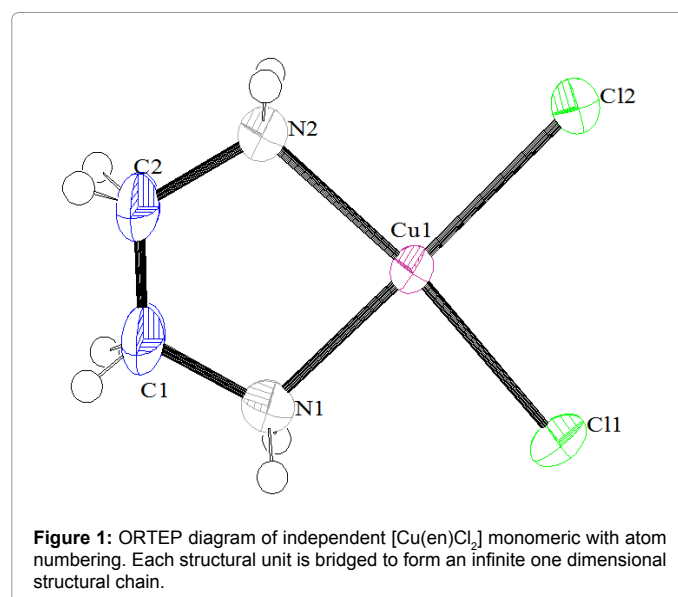
$$d_{norm} = \frac{d_i - r_i^{vdw}}{r_i^{vdw}} + \frac{d_e - r_e^{vdw}}{r_e^{vdw}} \quad (1)$$

Where,  $r_i^{vdw}$  and  $r_e^{vdw}$  are the van der Waals radii of the appropriate atoms which are internal and external to the surface, respectively. The value of  $d_{norm}$  is negative or positive when intermolecular contacts are shorter or longer than  $r^{vdw}$ , respectively. When  $d_{norm}$  is mapped on the Hirshfeld surface, close intermolecular distances are characterized by three identically colored regions: red regions stand for closer contacts and negative  $d_{norm}$  value, blue regions represent longer contacts and positive  $d_{norm}$  value and white regions correspond to the distance of contacts which is exactly the  $vdw$  separation and with a  $d_{norm}$  value of zero. The combination of  $d_e$  and  $d_i$  in the form of a 2D fingerprint plot [36,37] afford summary of intermolecular contacts in the crystal [38].

## Results and Discussion

### Description of the structure and Hirshfeld surface analysis

**Structure description:** Analysis of the X-ray data of  $\{[Cu(en)Cl_2]_n\}$ , reveals a structural linear chain. An ORTEP diagram of a chain fragment is illustrated in Figure 1. The bridging network consists of copper (II) ions bridged by chloride ligands to form a 'ladder type' linear chain (Figure S2) this compound is structurally similar to the analogous Cu complex [39,40]. The Cu(II) ion adopted hexacoordinated environment in a distorted octahedral geometry where the equatorial plan is formed by the first nitrogen atom provided by the (en) ligand, N<sub>2</sub>, with distance of 2.011(4) Å, and by three chlorine atoms which are triply bridging, Cl<sub>1</sub>, Cl<sub>1</sub><sup>i</sup> and Cl<sub>1</sub><sup>ii</sup>, with Cu-Cl distances are found to be Cu<sub>1</sub>-Cl<sub>1</sub>=2.2984(17) Å, Cu<sub>1</sub>-Cl<sub>1</sub><sup>i</sup>=2.885(3) and Cu<sub>1</sub>-Cl<sub>1</sub><sup>ii</sup>=2.885(3) Å, (symmetry element, i: 1-x, -1/2+y, 1-z; ii: 1-x, 1/2+y, 1-z) (Figure S3a). The axial positions of the octahedral geometry are occupied by one chlorine atom Cl<sub>2</sub> and the second nitrogen atom, N<sub>1</sub>, provided by the (en) ligand with the Cu<sub>1</sub>-Cl<sub>2</sub> is corresponding 2.2840(16) Å and the Cu<sub>1</sub>-N<sub>1</sub>=2.016 (4) Å. Selected bonds and angles are listed in Table S3. The distorted octahedral geometry of Cu(II) is confirmed by the Hirshfeld surface mapped over  $d_{norm}$  of Cu(II) (Figure 2). The Cu-Cu separation within the chain is 3.614 (1) Å which is



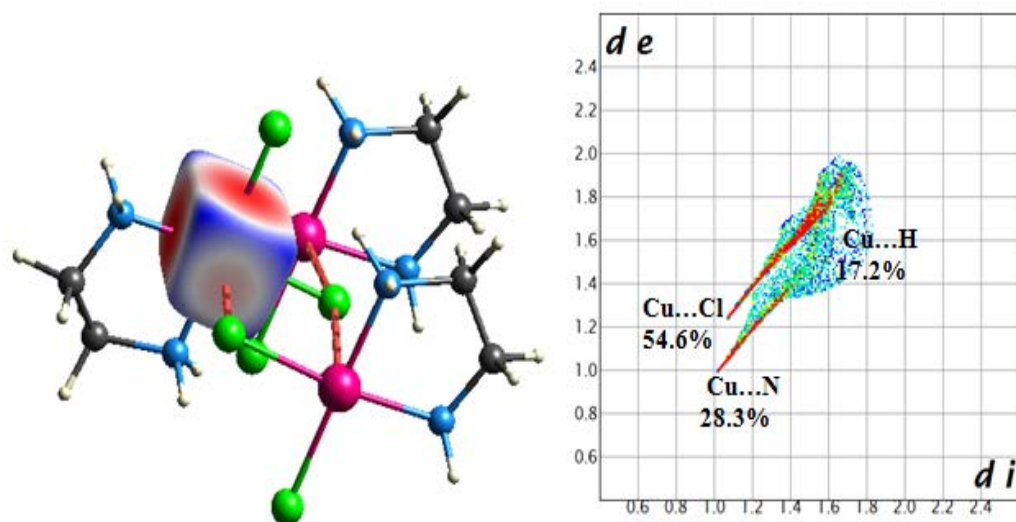


**Figure 2:** (a) Atomic Hirshfeld surface of Cu in  $\{[Cu(en)Cl_2]_n\}$  with the descriptor ' $d_{norm}$ ' mapped onto the surfaces. (b) Corresponding fingerprint plots for the metal atom.

comparable to the Cu...Cu separation in related Cu complexes [2,41]. The dihedral angle between the  $Cl_1...Cu(II)...Cl_1^i$  (red plan) and  $Cl_1^i-Cu(II)^{iii}-Cl_1$  (yellow plan) planes is  $10.07^\circ$  (Figure S3b) (symmetry code iii:  $x, -1+y, z$ ). The one-dimensional coordination polymeric chains are arranged parallel to one another, side by side in the *ab*-plan, connected between them by hydrogen bonds N-H...Cl, forming sheets parallel to the *ab*-plan (Figure 3). A variety of hydrogen bonds are established: inter-chain bonds, between adjacent chains in a sheet, and intra-chain bonds (Table 2).

The optimized geometry for the studied compound is presented in Figure 4. The values of the selected bond lengths and bond angles were compared to their calculated counterparts, and the results are summarized in Table S3. After careful comparison, we find that some of these geometric parameters are overestimated while the others are underestimated, which is not surprising given that the theoretical calculation belongs to the isolated molecule in the gaseous phase at 0K and the experimental result belongs to the molecule in the solid state with intermolecular interactions and crystal packing effect. This indicates that the calculation precision is satisfactory and the B3LYP/LanL2DZ level is suitable for the complex system studied here [42].

**Hirshfeld surface analysis:** The three-dimensional Hirshfeld surfaces of the complex  $\{[Cu(en)Cl_2]_n\}$  were analyzed so as to clarify the nature of the intermolecular interactions. 2D fingerprint plots reveal the contribution of those interactions in the crystal structure quantitatively, presenting the surfaces that have been mapped over a  $d_{norm}$  range of -0.246 to 1.515,  $d_e$  range of 0.889 to 2.539 and  $d_i$  range of 0.888 to 2.524 (Figure 5). It is clear that the presented information in Table 2 is clearly summarized in these spots, with the large circular depressions (deep red) visible on the views of the  $d_{norm}$  surfaces indicative of hydrogen-bonding contacts: H...Cl and Cl...H. Red regions on the  $d_e$  surface for title compound highlight the hydrogen bond acceptor Cl...H, where  $d_e$  is short, the  $d_e$  surface is close to the hydrogen nucleus outside the surface, but the hydrogen bond donor H...Cl is observed by the bright red area of  $d_i$  surface (Figure S4a). The proportion of Cl...H/H...Cl interactions comprises 34% and 20% of the total Hirshfeld surface of the complex, respectively. The Cl...H interactions

are represented by the spike  $d_i=1.655$  Å,  $d_e=0.898$  Å in the fingerprint plot (Figure S4a), and the H...Cl interactions are represented by the spike ( $d_i=0.898$  Å,  $d_e=1.655$  Å in the fingerprint plot, indicating amine H-atoms interacting with Cl atoms of anionic moiety for the formation of the supramolecular self-assembly. In addition to this, the H...H interactions (which appear where  $d_e=d_i=1$ ) have important weight in crystal structure, which is underlined by its high percentages, in the range from 35.7% relative to the total molecule area. The dominant H...H interactions are characterized by the bright red area of  $d_{norm}$  surface, as well as in the  $d_e$  and  $d_i$  surfaces (Figure S4b). The Figure 5a shows the Hirshfeld surfaces of the copper atom in the complex which have been mapped over  $d_{norm}$  surface. The deep red regions on the  $d_{norm}$  surface for Cu highlight the short Cu...Cl contact (the bond distances for Cu...Cl vary between 2.288 Å and 2.298 Å). The pale-red region on the  $d_{norm}$  surface display the large Cu...Cl contact (the bond distances for Cu...Cl equal 2.885 Å). Although the covalent bonding to chlorine and nitrogen atoms are dominant (see also the corresponding atomic fingerprint plots (Figure 5b), there are low contact patches which may be attributed to N-H...Cu interactions (H...Cu distances of the closest contacts range from 2.95-3.22 Å). The considered Cu atom exhibits up to 17.2% of contacts arising from N-H...Cu interaction on the atomic Hirshfeld surface, with 54.6% of the contacts arising from the coordinated Cl-Cu bonds and the remaining 28.3% of the contacts arising from the coordinated ethylenediamine -N-Cu bonds.

The Hirshfeld surface analysis clarifies the same results as X-ray crystal structure analysis and elucidates the intermolecular interactions in a new visual manner. The contributions of the variety of contacts exhibited by the complex  $\{[Cu(en)Cl_2]_n\}$  have been depicted in Figure S5.

**Crystal voids calculation:** The Figure S6 shows the voids in the crystal structure of  $\{[Cu(en)Cl_2]_n\}$  crystal voids are calculated using the program Crystal Explorer, which is based on the sum of spherical atomic electron densities at the appropriate nuclear positions (procrystal electron density). The crystal voids calculation results under 0.002 a.u. isovalue (1 a.u. of electron density =  $6.748 e \text{ \AA}^{-3}$ ), shows that the void volume of our compound in the order of  $13.81 \text{ \AA}^3$  and surface area in the order of  $44.65 \text{ \AA}^2$ . Constantly with the porosity, the calculated void

Crystal data	
Empirical formula	C <sub>2</sub> H <sub>8</sub> Cl <sub>2</sub> CuN <sub>2</sub>
Formula weight	194.55
Crystal system	Monoclinic
Space group	<i>P</i> 2 <sub>1</sub> / <i>m</i>
Unit cell dimension	
a (Å)	6.761 (5)
b (Å)	5.743 (5)
c (Å)	8.209 (5)
β (°)	93.737 (5) <sup>o</sup>
V (Å <sup>3</sup> )	318.1 (4) Å <sup>3</sup>
Z	2
D <sub>calc</sub> (Mg cm <sup>-3</sup> )	1.990
Absorption coefficient (mm <sup>-1</sup> )	4.07
F(000)	240
Crystal dimensions (mm <sup>3</sup> )	0.5 × 0.3 × 0.2
Crystal form; color	Prism; blue
θ range for data collection (°)	θ <sub>min</sub> = 2.5 θ <sub>max</sub> = 26.0
Summary of Data CCDC	1403872
Data	Collection
Reflections collected	3232
Independent reflections	694
Reflections with I > 2σ(I)	656
Limiting indices (hkl)	h = -8 → 8 k = -7 → 7 l = -10 → 10
T <sub>min</sub> T <sub>max</sub>	0.021 0.227
CCD area detector diffractometer	sealed tube graphite monochromator
radiation source:	φ and ω scans
Absorption correction	Multi-scan
Refinement	
R [F <sup>2</sup> > 2σ(F <sup>2</sup> )]	0.025
wR (F <sup>2</sup> )	0.068
Goodness-of-fit (GOF) on F <sup>2</sup>	S = 1.14
Data/restraints/parameters	694/0/43
Extinction coefficient	0.0023
Δρ <sub>min</sub> (e Å <sup>-3</sup> )	-1.08
Δρ <sub>max</sub> (e Å <sup>-3</sup> )	0.56

Table 1: Crystal data and structure refinement for [Cu(en)]Cl<sub>2</sub>.

D—H...A	D—H	H...A	D...A	D—H...A
N1—H1...Cl <sup>2i</sup>	0.90	2.81	3.680 (4)	163
N1—H2...Cl <sup>2i</sup>	0.90	2.81	3.680 (4)	163
N2—H7...Cl <sup>2ii</sup>	0.90	2.63	3.466 (4)	155
N2—H8...Cl <sup>2iv</sup>	0.90	2.63	3.466 (4)	155

Symmetry codes: (i) -x+1, y-1/2, -z+1; (ii) -x+1, y+1/2, -z+1; (iii) -x, y+1/2, -z+1; (iv) -x, y-1/2, -z+1.

Table 2: Hydrogen bonding distances (Å) and angle (°).

volume of our compound is 4.34%. There are no large cavities. We note that the electron-density isosurfaces are not completely closed around the components, but are open at those locations where interspecies approaches are found, e.g., N-H...Cl and N-H...Cu.

**Electrostatic potential, total electron density and molecular electrostatic potential:** The Figures 6a-6c shows the electrostatic potential ESP, the contour of electrostatic potential, electron density ED, contour of electron density and the molecular electrostatic potential MEP map figures for the title complex. The ED isosurface indicates that charge density is equally distributed in the plans of title

molecule. However, it can be seen from the ESP figures, that while the negative ESP regions are located around the chlorine atoms and reflected as a yellowish blob, the positive ESP is localized on the rest of the molecules. This result is expected, because ESP correlates with electro-negativity and partial charges.

The MEP provides a visual method to understand the relative polarity of the molecule. It is a plot of electrostatic potential mapped into the constant electron density surface. In order to understand sites for electrophilic attack and nucleophilic reactions as well as hydrogen-bonding interactions [43], MEP studies were carried out with the same method and basis set that were used for geometry optimization (B3LYP using LanL2DZ basis set). A visual representation of the chemically active sites such as the negative (red) regions of the MEP which are related to electrophilic reactivity and the positive (blue) regions which are associated with nucleophilic reactivity, as shown in Figure 6c. Potential increases in the order red < orange < yellow < green < blue. The color code of these maps ranges between -0.06394 a.u. (deepest red) and 0.06394 a.u. (deepest blue) in the compound. As can be seen in the Figure 6c, the negative regions are mainly localized in the chlorine atoms, with a maximum value of -0.06394 a.u. However, the maximum positive region is mainly over the amino atoms N, which can be considered as a possible site for nucleophilic attack, with a maximum value of 0.06394 a.u. This results supply information about the region from which the compound can have intra and intermolecular interaction.

## Vibrational studies

To gain more information on the crystal structure, we have undertaken a vibrational study using Infrared spectroscopy and Raman scattering. The theoretical and experimental vibrational spectra are shown in Figures S7 and S8. The assignments of the observed bands were essentially based on comparisons with calculated values for normal vibrations and previously reported data for similar compounds [44-46].

The experimental and calculated vibrational frequencies as well as corresponding assignments are presented in Table S4. Correlation graphics are presented in Figure S9 in order to compare the calculated vibrational frequencies with the experimental counterparts of [Cu(en)]Cl<sub>2</sub> compound. The corresponding fitting factors of those are 0.99831 (infrared) and 0.99941 (Raman). The experimental values prove to be in a good agreement with the calculated vibrational frequencies.

## The vibrations of ethylenediamine cations

The observed bands between 400 and 4000 cm<sup>-1</sup> are assigned to internal modes of organic cation. Numerous functional groups and skeletal groups such as: NH<sub>2</sub>, CH<sub>2</sub>, C-C, C-N and C-C-N are presented in ethylenediamine cation. These groups are manifested in IR and Raman spectra in different range with different intensities.

**Vibration of NH<sub>2</sub> groups:** The N-H stretching vibration appears strongly and broadly in region 3450-3300 cm<sup>-1</sup> [47]. For the title compound, a very strong band at 3300 cm<sup>-1</sup> and 3228 cm<sup>-1</sup> in the FT-IR spectrum are assigned as stretching N-H modes. The calculated values for this mode are 3490.64 cm<sup>-1</sup> and 3353.93 cm<sup>-1</sup>, respectively. Then, only four medium bands located at 2939.93, 2370.40, 2331.28 cm<sup>-1</sup> in the IR spectrum and 2961.7 cm<sup>-1</sup> in the Raman spectrum are observed. We have assigned all these bands to N-H stretching mode. As the N-H group of the (NH<sub>2</sub>) is involved in hydrogen bonds, the wavenumbers of this mode shifted towards lower values. In fact, the XRD study of the title compound reveals that each of the two hydrogen atoms in (NH<sub>2</sub>) moiety is involved in N-H...Cl hydrogen bonds with the lengths of

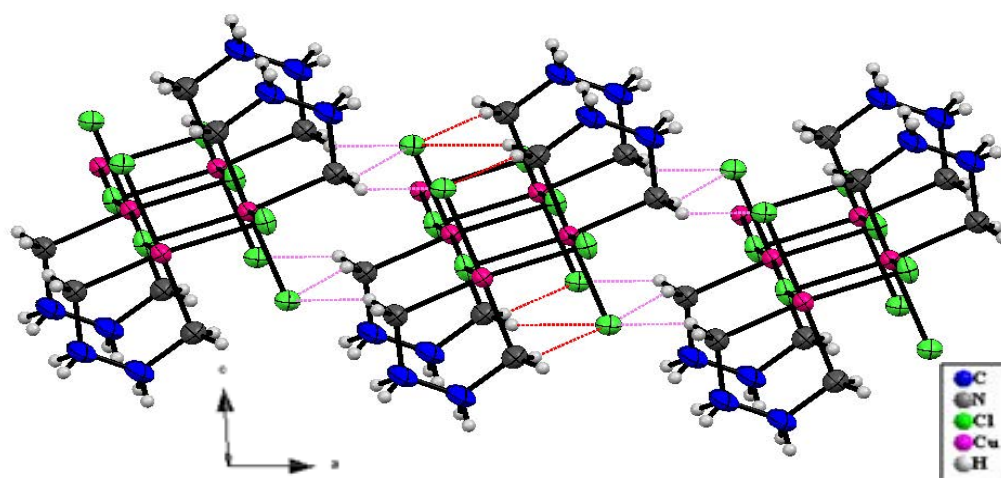


**Figure 3:** Sheet of compound  $\{[Cu(en)]Cl_2\}_n$  parallel to the *ab* plan. Hydrogen bonds indicated by different colors of dashed lines: (red for intra-chain N-H...Cl and violet for inter-chain N-H...Cl).

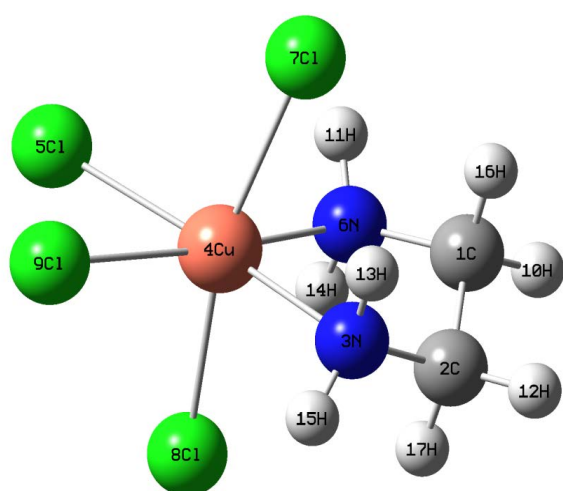


**Figure 4:** B3LYP/LanL2DZ optimized geometry of  $[Cu(en)]Cl_2$ .

the order 2.63 to 2.81 Å. Thus, one can expect various stretching N-H modes from 3300 to 2300  $cm^{-1}$  depending on the strength of hydrogen bonds. The shoulder IR band observed at 1660.18  $cm^{-1}$  is assigned to the asymmetric  $\delta_{as}(NH_2)$  bending mode. The corresponding predicted theoretically value is at 1559.42  $cm^{-1}$ . Strong infrared band at 1571.41  $cm^{-1}$  with its weak Raman counterpart at 1562.8  $cm^{-1}$  were attributed to the symmetric  $\delta_s(NH_2)$  bending mode. The DFT calculation gives its position at 1593.41  $cm^{-1}$ . The wagging and the torsional modes related to  $(NH_2)$  were observed and assigned.

**Vibration of  $CH_2$  groups:** The asymmetric stretching ( $\nu_{as}(CH_2)$ ), symmetric stretching ( $\nu_s(CH_2)$ ), scissoring ( $\nu_{sciss}(CH_2)$ ), wagging ( $\nu_w(CH_2)$ ) and twisting ( $\nu_t(CH_2)$ ) vibrations of  $CH_2$  groups are usually observed in the general order:  $\nu_{as}(CH_2) > \nu_s(CH_2) > \nu_{sciss}(CH_2) > \nu_w(CH_2) > \nu_t(CH_2)$  [47]. Their frequencies are observed in the following regions 3050  $\pm$  50, 2965  $\pm$  30, 1455  $\pm$  55, 1350  $\pm$  85, 1290  $\pm$  45 and 890  $\pm$  55  $cm^{-1}$ , respectively [48-50]. In our case, the  $CH_2$  asymmetric stretching vibrations are observed in IR spectrum as weak bands at 3100  $cm^{-1}$  and

at 3047.18  $cm^{-1}$  theoretically. The  $CH_2$  symmetric stretching mode is observed in IR spectrum at 2881.25  $cm^{-1}$  as weak band and at 2892.42  $cm^{-1}$  in Raman spectrum. The theoretically calculated values are 2935.47 and 2947.99  $cm^{-1}$ . The  $CH_2$  scissoring mode is located experimentally at 1457  $cm^{-1}$  in Infrared spectrum whereas its theoretical value is found at 1455.9  $cm^{-1}$ . The  $CH_2$  wagging mode appears at 1366.5  $cm^{-1}$  in Raman spectrum and predicted theoretically at 1368.76  $cm^{-1}$ . The observed wavenumber in the FT-IR spectrum at 1270.47  $cm^{-1}$  and 1123  $cm^{-1}$  and in Raman spectrum at 1109.82  $cm^{-1}$  are assigned to  $CH_2$  twisting mode while the theoretically computed values are observed at 1284.55  $cm^{-1}$  and 1225.06  $cm^{-1}$ . It is significant to note that the vibrational mode  $CH_2$  groups do not deviate much from their expected values, suggesting that the interaction of these groups with the environment is not strong.

**Vibrations of C-N, C-C and C-C-N groups:** The Raman band observed at 1063.63  $cm^{-1}$  and calculated at 1077.42  $cm^{-1}$  can be attributed to C-N stretching mode. The weak intensity band observed at 977  $cm^{-1}$  in IR spectrum and calculated at 1008.57  $cm^{-1}$  is assigned to C-C stretching mode. The C-C-N in plan bending modes is observed at 471  $cm^{-1}$  in IR spectrum and at 475  $cm^{-1}$  in Raman spectrum and proved by DFT calculation at 471.34  $cm^{-1}$ .

In the case of the external vibrations of Cu-N, Cu-Cl and Cl-Cu-Cl groups: the asymmetric and symmetric stretching of Cu-Cl appeared at 303, 254.4 and 213.6  $cm^{-1}$  in Raman spectrum. The DFT calculations yielded those modes at 287.93, 255.75 and 220.19  $cm^{-1}$ , respectively. The corresponding Cu-N stretching vibration has been nearly identified 377  $cm^{-1}$  for Raman while the theoretically computed values are observed at 342.48  $cm^{-1}$ . The Cl-Cu-Cl scissoring and bending vibrations are identified at 161 and 92.77  $cm^{-1}$  for Raman. The theoretically calculated values are 181.04 and 93.5  $cm^{-1}$ , respectively.

### Mulliken population analysis

The Mulliken populations indicated the charge distributions over the atoms. The Mulliken atomic charge quantifies how the electronic structure changes under atomic displacement, it therefore affects dipole moment, molecular polarizability, electron structure, acidity-basicity behaviour and a lot of other properties of molecular systems [51].

Mulliken atomic charges of  $[Cu(en)]Cl_2$  molecule have been calculated using B3LYP method at LanL2DZ basis and shown in

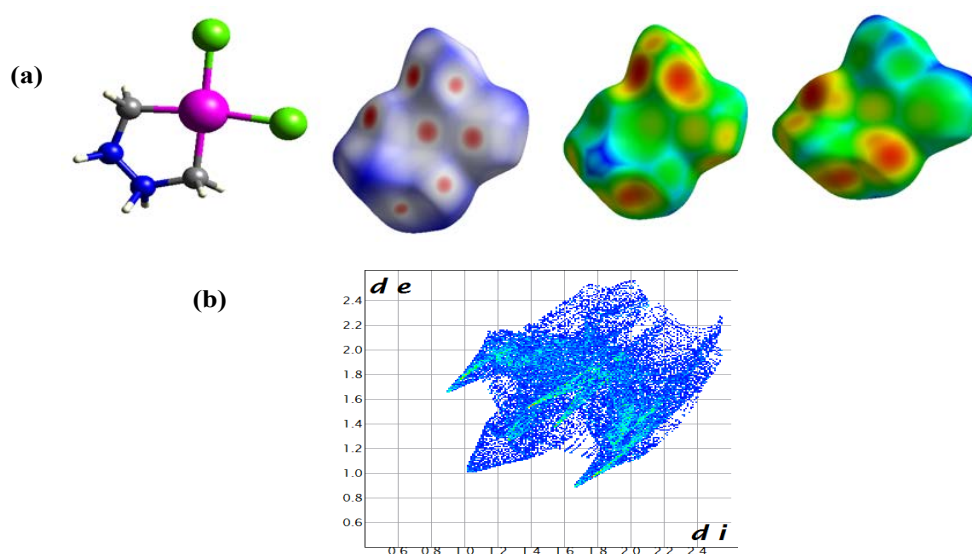


**Figure 5:** (a) Hirshfeld surfaces of the complex [Cu(en)]Cl<sub>2</sub>, the Hirshfeld surface is shown mapped with  $d_{\text{norm}}$  (left),  $d_e$  (center) and  $d_i$  (right). The ball-and-stick representation of this molecule is given to the left of the surfaces. (b) Fingerprint plots: Full into different intermolecular interactions within the compound.

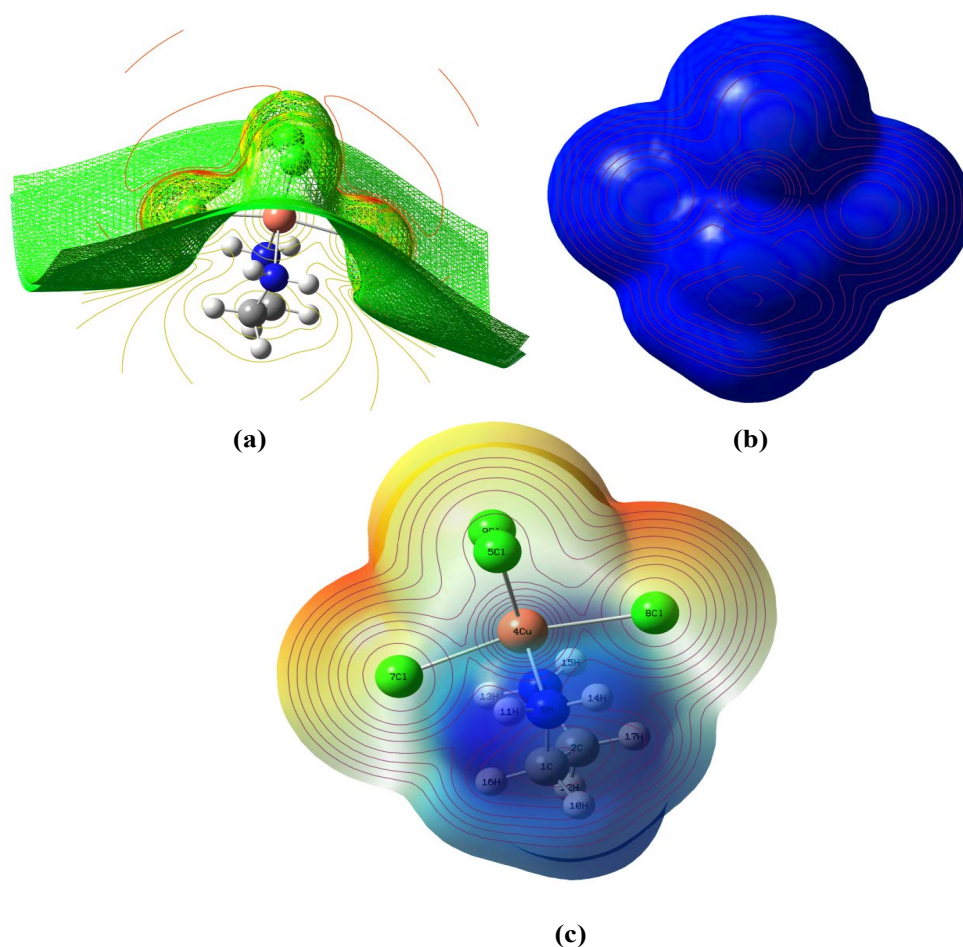


**Figure 6:** Molecular surfaces of optimized geometry of [Cu(en)]Cl<sub>2</sub>, (a) Electrostatic potential (ESP), (b) Total Electron Density (ED) and (c) Molecular Electrostatic Potential (MEP).

Figures S10 and S11. The charge distribution of  $[\text{Cu}(\text{en})]\text{Cl}_2$  shows that the carbon atoms are negative. This is due to the presence of hydrogen atoms [52]. All hydrogen atoms are positively charged. Moreover, Mulliken atomic charges also show that the H atoms attached to N have bigger positive atomic charges (0.385e and 0.376e) than the other hydrogen atoms. This is due to the presence of electronegative nitrogen atoms which withdrew electrons from H atoms. The nitrogen atoms have the higher negative charges (-0.600e). This may refer to the fact that the nitrogen atoms have withdrawn electrons from C, H and Cu atoms. Cl7/Cl8 chlorine atoms have the high negative charges (-0.315e) while the other chlorine atoms have less negative charges (-0.075e). This result reveals that there is charge transfer through the hydrogen bonds (N-H...Cl). The high negatively charges are noticed for chloride Cl7 and Cl8, which are involved, as acceptor, in hydrogen bonds.

### Optical properties

The Figure 7 shows the optical absorption spectrum of  $[\text{Cu}(\text{en})]\text{Cl}_2$  film measured at room temperature. As it can be seen, two kinds of optical absorption bands are observed. The first is a strong absorption band at 340 nm, the second is a large band located at 650 nm. We performed theoretical TD-DFT calculations to understand the electronic structure and assign the observed absorption bands. The B3LYP Hamiltonian was selected because it was proven to provide accurate structures and reasonable UV-vis. spectra for a variety of chromophores [53] including organometallic complexes [54-56]. As

seen in Figure 7 the calculated and experimental optical spectra display an acceptable agreement for the title compound. The assignment of the excitation energies to the experimental bands was performed on the basis of energy values and oscillator strength in Table 3. We listed the singlet excited states with oscillator strength higher than 0.09 along with assignments of the major contributing electronic transitions. The normalized contribution percentage of the major contributing electronic transitions contributing to the Singlet excited states were given in parentheses. The spatial distributions of the molecular orbital participating in these transitions and the energy level diagrams are shown in Figure 8. The performed calculations indicated an intense electronic transition at 388 nm. They agree with the optical absorption band observed at 340 nm. This band corresponds to electronic transition from the highest occupied molecular orbital ( $\beta\text{HOMO-8}$ ) to the lowest unoccupied molecular orbital ( $\beta\text{LUMO}$ ) and ( $\beta\text{HOMO-9}/\beta\text{HOMO-12}$ ) to ( $\beta\text{LUMO}$ ). The HOMO-8, HOMO-9 and LUMO are localized in the inorganic part. This absorption band must be assigned to Ligand to Metal Charge Transfer (LMCT) and/or to Metal to Ligand Charge Transfer (MLCT) transition [57,58].

The electronic transition at 682 nm is in good agreement with the second observed absorption band existing at 650 nm. This band corresponds to electronic transitions from the  $\beta\text{HOMO3}/\beta\text{HOMO}$  to  $\beta\text{LUMO}$ . This band must be assigned to the d-d transitions composed from orbits of Cu(II) [59,60].

$\lambda$ (nm)		f	Assignment (Major contributions)	Character
$\lambda_{\text{exp}}$	$\lambda_{\text{calc}}$			
340 (3.64 eV)	388	0.14	H-12( $\beta$ ) $\rightarrow$ L+1( $\beta$ ) (10%) H-9( $\beta$ ) $\rightarrow$ L+1( $\beta$ ) (44%) H-8( $\beta$ ) $\rightarrow$ L ( $\beta$ ) (17%)	LMCT and/or MLCT
650 (1.90 eV)	682	0.10	H-3( $\beta$ ) $\rightarrow$ L ( $\beta$ ) (63%) H( $\beta$ ) $\rightarrow$ L ( $\beta$ ) (16%)	d-d

$\lambda$ : Wavelength, H: HOMO, L: LUMO

**Table 3:** Calculated wavelengths ( $\lambda_{\text{max}}$ ), oscillator strengths ( $f > 0.09$ ), main orbital transition contributions of absorption spectra of  $[\text{Cu}(\text{C}_2\text{H}_8\text{N}_2)]\text{Cl}_2$  complex using TDDFT as well as their character and related experimental values.

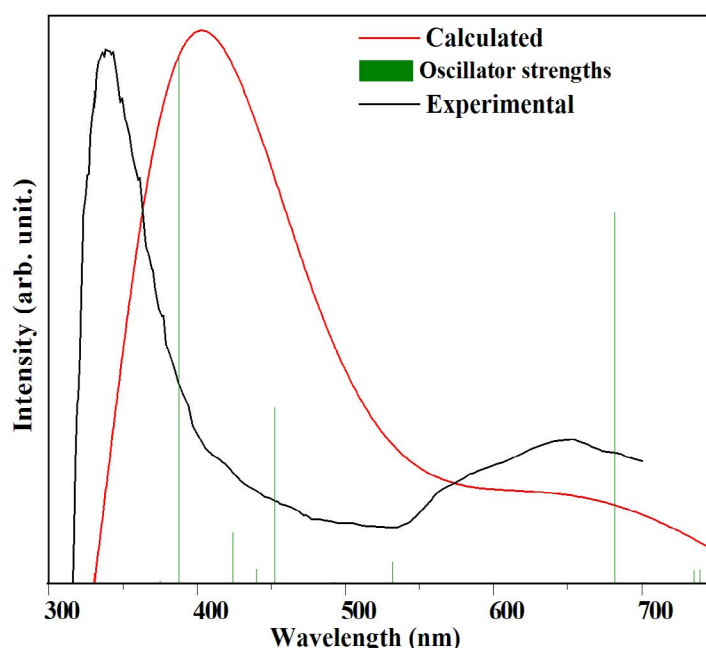


**Figure 7:** Experimental (black) calculated (red) UV-Visible spectra of  $[\text{Cu}(\text{en})]\text{Cl}_2$  and oscillator strengths are shown as green vertical lines.

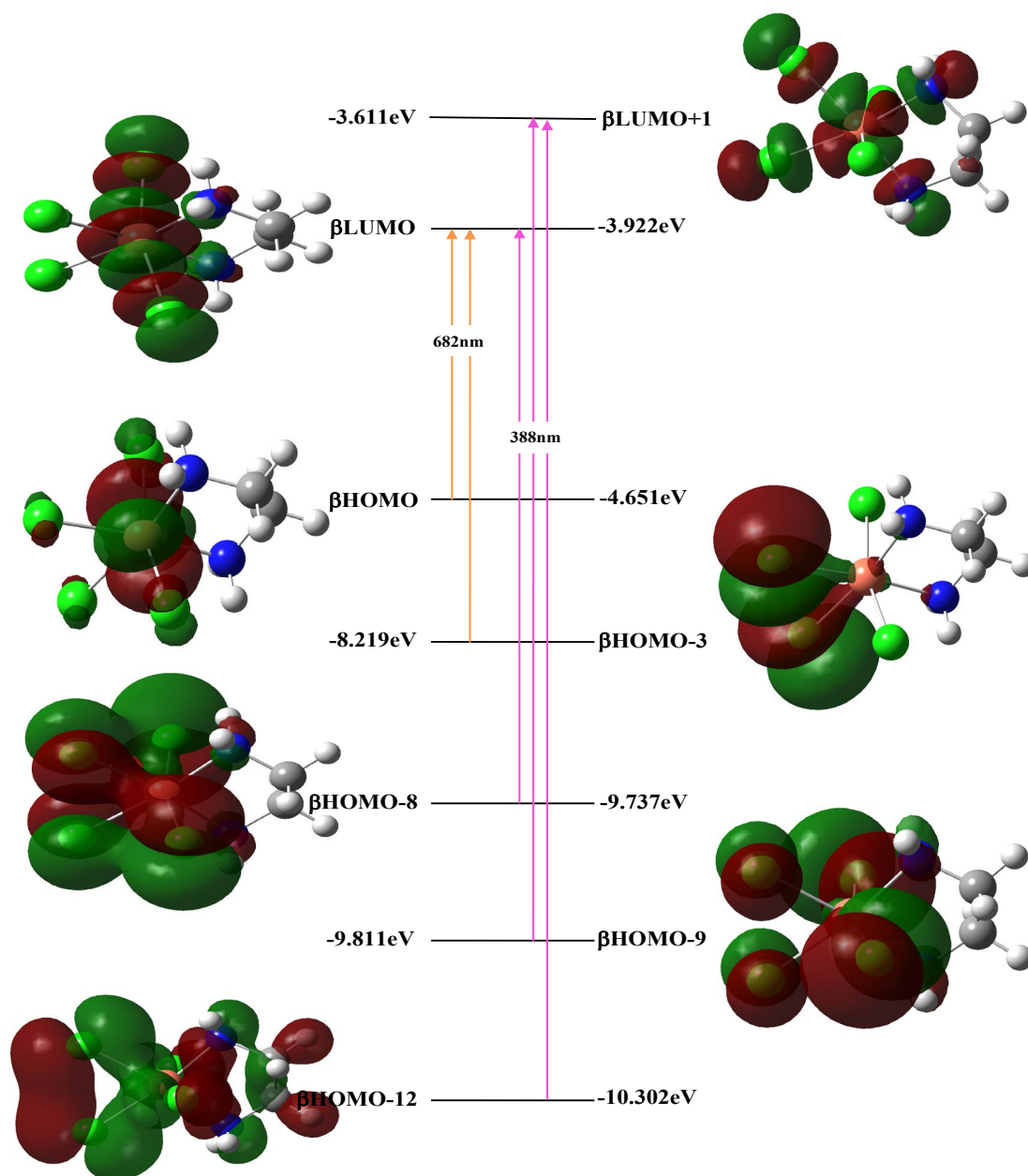


Figure 8: TDDFT-calculated electronic transitions in complex  $[\text{Cu}(\text{en})]\text{Cl}_2$ .

## Conclusions

Dichlorocuprate based complex having general formula  $[\text{Cu}(\text{en})]\text{Cl}_2$  that exhibits a one dimensional structure has been synthesized under hydrothermal conditions. The X-ray diffraction analysis revealed the molecular arrangements and the formation of hydrogen bonds in the crystal. The Hirshfeld surface computational method allows us to examine the intermolecular interaction of the title compound. The optimized molecular structure, electronic properties, vibrational frequencies and intensity of vibrations of the title compound are calculated by DFT method using B3LYP method at LanL2DZ basis levels. The optimized geometric parameters (bond lengths and bond angles) are theoretically determined by DFT theory and compared

with the experimental data. The vibrational wavenumber, FT-IR and FT-Raman intensities were calculated and were found in very good agreement with experimental vibrations. The MEP map of  $[\text{Cu}(\text{en})]\text{Cl}_2$  shows that the negative potential sites are on chlorine atoms and the positive potential sites are around the hydrogen atoms. The Mulliken populations indicated the charge distributions over the atoms. The calculated HOMO and LUMO energies help to exemplify the chemical reactivity and kinetic stability of the molecule.

## Acknowledgements

The authors would like to thank the members of units of common services, in particular Mr Tarek Gargouri, at the University of Sfax for their assistance for the measurements of X-ray diffraction.

## References

- Zdanowska-Fraćzek M, Holderna-Natkaniec K, Fraćzek ZJ, Jakubas R (2009) Molecular dynamics and electrical conductivity of  $(C_3N_2H_5)_5Bi_2Cl_{11}$ . Solid State Ionics 180: 9-12.
- Gómez V, Benet-Buchholz J, Martín E, Galán-Mascarós JR (2014) Architectures in Copper Metal-Organic Frameworks from 4-Substituted Anionic 1, 2, 4-Triazoles. J Inorg Chem 2014: 3125-3132.
- Bandyopadhyay S, Das A, Mukherjee GN, Cantoni A, Bocelli G, et al. (2004) Synthesis, X-ray crystal structures, physicochemical and magnetic studies on copper (II) N-(2-carboxyphenyl) iminodiacetate polymers. Polyhedron 23: 1081-1088.
- Lehle A, Beghidja A, Beghidja C, Welter R, Kurmoo M, et al. (2015) Synthesis, structures and magnetic properties of dimeric copper and trimeric cobalt complexes supported by bridging cinnamate and chelating phenanthroline. Comptes Rendus Chimie 18: 530-539.
- Bai ZS, Liu GX, Lu Y, Sun WY (2008) Preparation, structure, magnetic and photoluminescence properties of copper (II) and cadmium (II) frameworks with 4, 4'-bipyridine-2, 2', 6, 6'-tetracarboxylate. Inorg Chem Comm 11: 513-517.
- Chu Q, Liu GX, Okamura TA, Huang YQ, Sun WY, et al. (2008) Structure modulation of metal-organic frameworks via reaction pH: Self-assembly of a new carboxylate containing ligand N-(3-carboxyphenyl) iminodiacetic acid with cadmium (II) and cobalt (II) salts. Polyhedron 27: 812-820.
- Sheng YW, Wang Y, Okamura TA, Sun WY, Ueyama N (2007) Synthesis, crystal structure and nonlinear optical property of cadmium (II) and copper (II) complexes with novel chiral ligand. Inorg Chem Comm 10: 432-436.
- Cui FY, Ma XY, Li C, Dong T, Gao YZ, et al. (2010) Two new organic-inorganic hybrid compounds based on metal-pyrazine coordination polymers and Keggin polyoxometalates: effect of metal ions on the structure. J of Solid State Chem 183: 2925-2935.
- DeBurgomaster P, Zubieta J (2010) Organic-inorganic hybrid materials: Ligand influences on the structural chemistry of copper-vanadates. Inorg Chimica Acta 363: 2912-2919.
- Colombo A, Dragonetti C, Roberto D, Valore A, Biagini P, et al. (2013) A simple copper (I) complex and its application in efficient dye sensitized solar cells. Inorg Chimica Acta 407: 204-209.
- Tamuly C, Barooah N, Batsanov AS, Katakya R, Baruah JB (2005) Structural and spectroscopic properties of bis-3-picolinium 1, 8-naphthalimide tetrachlorocuprate. Inorg Chem Comm 8: 689-691.
- Ozaydin C, Akkilic K (2014) Electrical and photoelectrical properties of copper (II) complex/n-Si/Au heterojunction diode. American Journal of Optics and Photonics 2: 69-74.
- Mistri S, Bertolasi V, Manna SC (2015) Bis-chelated-(3-methoxy-2-oxo-benzaldehyde)-copper (II) complex: Synthesis, crystal structure, fluorescence property, DFT calculation, and catecholase activity. Polyhedron 88: 101-109.
- Wu H, Yun R, Wang K, Li K, Huang X, et al. (2010) Synthesis and characterization of the ligand based on benzimidazole and its copper complex: DNA binding and antioxidant activity. Allg Chem 636: 1397-1400.
- Uedga K, Goto M, Sugimoto T, Endo S, Toyota N, et al. (1997) Synthesis, and electrical conducting and magnetic properties of a neutral bis (dimethylthiotetrafulvalenyldithiolate) copper complex. Synthetic Metals 85: 1679-1680.
- Busi S, Lahtinen M, Valkonen J, Rissanen K (2006) Crystal structures and thermal behavior of bis [dibenzyltrimethylammonium]  $CuBr_4$ , bis [dibenzyltrimethylammonium]  $CuCl_4$  and bis [dimethyl (2-phenylethyl) ammonium]  $CuBr_4$  crystallized from acetonitrile and dilute HX (X= Cl or Br) solutions. J of Mol Struct 794: 277-287.
- Das A, Dey B, Jana AD, Hemming J, Helliwell M, et al. (2010) Effect of protonated aminopyridines on the structural divergences of M (II)-malonate complexes (M=Cu, Ni, Co). Polyhedron 29: 1317-1325.
- Zhu HB, Wu YF, Zhang G, Lou YB, Hu J (2015) Side-chain-modulated supramolecular assembly between  $CuX_2$  (X=Cl, Br) and quasi-planar  $\pi$ -conjugated organic synthons of 1, 3, 5-tris (2-alkylthiopyrimidinyl). Polyhedron 85: 60-68.
- Patil YP, Nethaji M (2015) Synthesis and crystal structure of copper (II) uracil ternary polymeric complex with 1, 10-phenanthroline along with the Hirshfeld surface analysis of the metal binding sites for the uracil ligand. J of Mol Struct 1081: 14-21.
- Dai J, Xu J (2011) Acta Cryst E 67: 170-170.
- Du ZX, Li JX, Han RQ (2011) Syntheses, Characterizations and Crystal Structures of Two Copper Coordination Polymers Both Having  $Cu_2Cl_2$  Bridging Subunit  $[Cu(bipy)_{1/2}Cl]_n$  (1) and  $\{[(CuII)_4(phen)_4(SSA)_2Cl_2](H_2O)_2(DMF)_2]_n\}$  (2). J Chem Crystallogr 41: 34-38.
- Baccar I, Issaoui F, Zouari F, Hussein M, Dhahri E, et al. (2010) Magneto-structural studies of the bis (1, 4-bis (3-aminopropylamine) piperazinium) chloride pentachlorocuprate (II) trihydrate. Solid State Comm 150: 2005-2010.
- Weng DF, Wang BW, Wang ZM, Gao S (2011) Polymorphism of  $(H_2mela)_2[CuCl_2]Cl$  (mela= melamine): structures, transformation and magnetic properties. Cryst Eng Comm 13: 4683-4683.
- Kumara R, Obraia S, Joshib VK, Kumarb V, Shahab S (2015) Computational, crystal structure and antimicrobial studies of directly synthesized dichloroethylenediaminecopper (II) complex. Commun Inorg Synth 3: 9-15.
- Sheldrick GM (1990) Phase annealing in SHELX-90: direct methods for larger structures. Acta Cryst 46: 467-473.
- Sheldrick GM (1997) Program for Crystal Structure Refinement. University of Gottingen, Germany.
- Macrae CF, Bruno IJ, Chisholm JA, Edgington PR, McCabe P, et al. (2008) Mercury CSD 2.0—new features for the visualization and investigation of crystal structures. J Appl Crystallogr 4: 466-470.
- Crystal Maker Software (1999) Crystal Maker. Version 4.4. Crystal Maker Software, Bicester, England.
- Frisch MJ, Trucks GW, Schlegel HB, Scuseria GE, Robb MA, et al. (2004) Gaussian 03. Revision E.01, Gaussian, Inc., Wallingford, CT.
- Becke AD (1993) Density-functional thermochemistry. III. The role of exact exchange. J Chem Phys 98: 5648-5652.
- Hay PJ, Wadt WR (1985) Ab initio effective core potentials for molecular calculations. Potentials for the transition metal atoms Sc to Hg. J Chem Phys 82: 270-283.
- Hay PJ, Wadt WR (1985) Ab initio effective core potentials for molecular calculations. Potentials for K to Au including the outermost core orbitals. J Chem Phys 82: 299-310.
- Rauhut G, Pulay P (1995) Transferable scaling factors for density functional derived vibrational force fields. J Phys Chem 99: 3093-3100.
- Dennington R, Keith T, Millam J (2009) GaussView, Version 5, Semichem Inc., Shawnee Mission KS.
- Luo YH, Mao QX, Sun BW (2014) Two new complexes with 6-methylnicotinic acid ligand: Synthesis, crystal structure and Hirshfeld surfaces. Inorg Chimica Acta 412: 60-66.
- Spackman MA, McKinnon JJ (2002) Fingerprinting intermolecular interactions in molecular crystals. Cryst Eng Comm 4: 378-392.
- Rohl AL, Moret M, Kaminsky W, Claborn K, McKinnon JJ, et al. (2008) Hirshfeld surfaces identify inadequacies in computations of intermolecular interactions in crystals: pentamorphic 1, 8-dihydroxyanthraquinone. Cryst Growth Des 8: 4517-4525.
- Barr PG, Dong W, Gilmore CJ, Jayatilaka D, McKinnon JJ, et al. (2007) Comparing entire crystal structures: structural genetic fingerprinting. Cryst Eng Comm 9: 648-652.
- Helis HM, Goodman H, Wilson RB, Morgan JA, Hodgson DJ (1977) A novel halogen-bridged system: synthesis and structures of dibromo [2-(2-aminomethyl) pyridine] copper (II) and dibromo (2-methyl-1, 2-diaminopropane) copper (II). Inorganic Chemistry 16: 2412-2416.
- Hernandez-Molina M, Gonzalez-Platas J, Ruiz-Pérez C, Lloret F, Julve M (1999) Crystal structure and magnetic properties of the single- $\mu$ -chloro copper (II) chain  $[Cu(bipy)Cl_2]_n$  (bipy= 2, 2'-bipyridine). Inorganica Chimica Acta 284: 258-265.
- Fariati I, Craig DC, Phillips DJ (1998) Inorganica Chimica Acta 268: 135-140.
- Hay PJ, Wadt WR (1985) Ab initio effective core potentials for molecular calculations. Potentials for the transition metal atoms Sc to Hg. J Chem Phys 82: 270-283.

43. Mansour AM (2013) Molecular structure and spectroscopic properties of novel manganese (II) complex with sulfamethazine drug. *J of Mol Structure* 1035: 114-123.
44. Elleuch S, Feki H, Abid Y (2007) HF, MP2 and DFT calculations and spectroscopic study of the vibrational and conformational properties of N-diethylendiamine. *Spectrochimica Acta Part A: Mol and Biomol Spec* 68: 942-947.
45. Camí G, Villalba EC, Di Santi Y, Colinas P, Estiu G, et al. (2011) Synthesis, thermogravimetric, spectroscopic and theoretical characterization of copper (II) complex with 4-chloro-2-nitrobenzenesulfonamide. *J Mol Struct* 995: 72-77.
46. Staśkiewicz B, Turowska-Tyrk I, Baran J, Górecki C, Czaplą Z (2014) Structural characterization, thermal, vibrational properties and molecular motions in perovskite-type diaminopropanetetraclorocadmate  $\text{NH}_3(\text{CH}_2)_3\text{NH}_3\text{CdCl}_4$  crystal. *J of Phy and Chem Solids* 75: 1305-1317.
47. Samet A, Boughzala H, Khemakhem H, Abid Y (2010) Synthesis, characterization and non-linear optical properties of Tetrakis (dimethylammonium) Bromide Hexabromobismuthate:  $\{[(\text{CH}_3)_2\text{NH}_2]^+\}_4 \cdot \text{Br}^- [\text{BiBr}_6]^{3-}$ . *J of Mol Structure* 984: 23-29.
48. Karabacak M, Cinar Z, Kurt M, Sudha S, Sundaraganesan N (2012) FT-IR, FT-Raman, NMR and UV-vis spectra, vibrational assignments and DFT calculations of 4-butyl benzoic acid. *Spectrochim Acta A: Mol and Biomol Spec* 85: 179-189.
49. Roeges NPG (1994) *A Guide to the Complete Interpretation of Infrared Spectra of Organic Structures*. Wiley, New York.
50. Colthup NB, Daly LH, Wiberly SE (1975) *Introduction to Infrared and Raman Spectroscopy*. Academic Press, New York.
51. Mulliken RS (1955) Electronic population analysis on LCAO-MO molecular wave functions. II. Overlap populations, bond orders, and covalent bond energies. *J Chem Phys* 23: 1841-1846.
52. Guidara S, Ahmed AB, Abid Y, Feki H (2014) Molecular structure, NLO, MEP, NBO analysis and spectroscopic characterization of 2, 5-dimethylanilinium dihydrogen phosphate with experimental (FT-IR and FT-Raman) techniques and DFT calculations. *Spectrochimica Acta Part A: Mol and Biomol Spec* 127: 275-285.
53. Dreuw A, Head-Gordon M (2005) Single-reference ab initio methods for the calculation of excited states of large molecules. *Chemical Reviews* 105: 4009-4037.
54. Andzelm J, Rawlett AM, Orlicki JA, Snyder JF (2007) Optical properties of phthalocyanine and naphthalocyanine compounds. *J Chem Theory Comput* 3: 870-877.
55. Nemykin VN, Makarova EA, Grosland JO, Hadt RG, Kuposov AY (2007) Preparation, characterization, molecular and electronic structures, TDDFT, and TDDFT/PCM study of the solvatochromism in cyanovinylferrocenes. *Inorg Chem* 46: 9591-9601.
56. Santi S, Orian L, Donoli A, Durante C, Bisello A, et al. (2007) Charge Transfer through Isomeric Unsaturated Hydrocarbons. Redox Switchable Optical Properties and Electronic Structure of Substituted Indenes with a Pendant Ferrocenyl. *Organometallics* 26: 5867-5879.
57. Philip V, Suni V, Kurup MRP, Nethaji M (2006) Copper (II) complexes derived from di-2-pyridyl ketone N (4), N (4)-(butane-1, 4-diyl) thiosemicarbazone: Crystal structure and spectral studies. *Polyhedron* 25: 1931-1938.
58. Zareia SA, Khaledianb D, Akhtarid K, Hassanzadehe K (2015) Copper (II) and nickel (II) complexes of tetradentate Schiff base ligand: UV-Vis and FT-IR spectra and DFT calculation of electronic, vibrational and nonlinear optical properties. *Molecular Physics* 113: 3296-3302.
59. Ebrahimipour SY, Sheikhshoae I, Crochet A, Khaleghi M, Fromm KM (2014) A new mixed-ligand copper (II) complex of (E)-N'-(2-hydroxybenzylidene) acetohydrazide: Synthesis, characterization, NLO behavior, DFT calculation and biological activities. *J of Mol Struct* 1072: 267-276.
60. Gaye M, Sarr O, Sall AS, Diouf A, Hadabere S (1997) Infrared and UV-Vis studies of copper (II) complexes of 3, 6-bis ((saliclidenamino) ethyl)-sulfanylpiperazine. *Bull Chem Soc Ethiop* 11: 111-119.